Hindawi
Advances in Materials Science and Engineering
Volume 2022, Article ID 2325213, 13 pages
https://doi.org/10.1155/2022/2325213

Research Article

Synthesis Optimization of Activated Carbon Driven from Scrap Tire for Adsorbent Yield and Methylene Blue Removal under Response Surface Methodology

Estifanos Kassahun,[1,2] **Solomon Tibebu**,[3,4,5] **Yobsen Tadesse**,[2] **and Nigist Awish**[6]

[1]*Department of Chemical Engineering, College of Biological and Chemical Engineering, Addis Ababa Science and Technology University, Addis Ababa 16417, Ethiopia*
[2]*Food and Beverage Industry Research and Development Center, Addis Ababa, Ethiopia*
[3]*Department of Environmental Engineering, College of Biological and Chemical Engineering, Addis Ababa Science and Technology University, Addis Ababa 16417, Ethiopia*
[4]*Sustainable Energy Center of Excellence, Addis Ababa Science and Technology University, Addis Ababa 16417, Ethiopia*
[5]*Bioprocess and Biotechnology Center of Excellence, Addis Ababa Science and Technology University, Addis Ababa 16417, Ethiopia*
[6]*Ethiopian Conformity Assessment Enterprise, Addis Ababa, Ethiopia*

Correspondence should be addressed to Solomon Tibebu; solomon.tibebu@aastu.edu.et

Received 10 May 2022; Revised 15 June 2022; Accepted 6 August 2022; Published 22 August 2022

Academic Editor: Achraf Ghorbal

This study aimed to investigate the synthesis optimization of activated carbon-driven scrap tires for adsorbent yield and methylene blue removal under response surface methodology. The scrap tire sample was activated by KOH using ethanol as a solvent. The optimized activated carbon was characterized using proximate analysis, scanning electron microscope (SEM), X-ray diffraction (XRD), and Brunauer Emmett Teller (BET) method. The activated carbon was demineralized using 5 M NaOH + 98% H_2SO_4 (1 : 1) as a solvent to enhance the surface area. Langmuir, Freundlich, Temkin, and Dubinin-Radushkevich models were used to check the adsorption isotherm. The adsorption kinetics was checked using pseudo-first-order and pseudo-second-order models. Weber-Morris intraparticle diffusion model was used to study the diffusion mechanism. The optimum impregnation ratio, impregnation time, and carbonization temperature for synthesizing the activated carbon were 2 g/g, 12 hr, and 700°C, respectively. The moisture content, volatile matter, ash content, fixed carbon, and bulk density of the activated carbon were 6.13%, 9.42%, 5.34%, 79.11%, and 0.89 mg/L, respectively. The surface area of optimized activated carbon was enhanced by demineralization process and increased from 53 m^2/g to 260.26 m^2/g. Temkin adsorption isotherm with R^2 values of 0.982 and pseudo-second-order adsorption kinetics with R^2 values of 0.999 best fits the experimental data respectively. Intraparticle diffusion was not the only rate-controlling step for both optimized and demineralized ($NaOH + H_2SO_4$) activated carbon. It can be concluded that the optimized and demineralized activated carbon derived from scrap tires has a promising potential to be used as a low-cost adsorbent in developing countries including Ethiopia. However, further investigation needs to be conducted before scaling up at industrial level.

1. Introduction

Industries including textile, printing, plastic, cosmetic, paper, and food processing industries use dyes [1, 2]. There are over 100,000 different types of commercially available dye throughout the world. According to Fito et al. [3], 700,000 tons of dyes are globally produced per year. During the manufacturing process, approximately, 15% of the dyestuff is lost in industrial wastewater [4]. Wastewater that contains dyes is characterized by low biodegradability and high

organic matter concentration [5]. Discharging untreated wastewater that is contaminated by dye affects the health of both terrestrial and aquatic environments including soil, algae, fishes, and other living and non-living components of the environment [6]. Methylene blue is a cationic soluble dye that dissociates into cations and chloride ions [7]. It has various applications in dyeing industries, chemistry, biology, and medical science [8]. Methylene blue contaminated wastewater has both acute and chronic effects depending on the rate of exposure and its level of concentration in the wastewater. Among such acute and chronic effects allergic, dermatitis, skin irritation, cancer, and mutation are the major ones [9]. According to Patel et al. [10], photosynthesis can be prohibited by methylene blue dye that has a concentration of less than 1 mg/l. Therefore, treating this wastewater is mandatory to protect the environment from contamination [11].

Different conventional treatment techniques including physical, chemical, and biological methods have been used to treat wastewater containing dye contaminants [12]. However, advanced wastewater treatment technologies are becoming preferable to effectively and efficiently remove dye from wastewater [13]. Due to its simplicity of design, ease of operation, high ability to remove different pollutants, and high efficiency, adsorption is preferred to remove dye over other advanced wastewater treatment technologies [14].

Among different adsorbents, activated carbon is widely used to treat water and wastewater [15]. Moreover, activated carbon is used in air pollution treatment [16]. Commercial activated carbon is well known for its high surface area and adsorption capacity. However, these adsorbents are expensive; therefore, they are not recommended for developing countries including Ethiopia [17, 18].

To resolve this challenge, research is being conducted by different scholars in investigating eco-friendly and low-cost precursors for activated carbon [19, 20]. Peanut shell, sawdust, bagasse, and bamboo are some of the activated carbon precursors that have been studied previously [21, 22].

Around 1.5 billion scrap tires per year are disposed of in the environment [23]. According to Ali et al. [24], in the coming years, it is expected that 20 million additional scrap tires will be disposed of per year. Big cities are the main disposal sites for scrap tires [2]. The main contributors to the increment of scrap tires are trucks, vehicles, motorcycles, and bicycles [25]. In developing countries such as Ethiopia, the amount of scrap tires is expected to increase along with the increase of vehicles [26]. According to Alamrew [27], annually, 40,175 tons of scrap tires are generated in Ethiopia. Scrap tires are causing adverse environmental impacts [28]. Energy recovery through combustion and disposal in landfills are the two common methods that are being used to manage this waste [29]. However, these methods have both environmental and health impacts.

The release of chemicals into the atmosphere is the main health concern that results from combustion [30]. When they are dumped in landfills, they can also cause a negative impact on hygiene by being a breeding ground for mosquitoes and insects [24]. Due to the leaching of trace metals, sulfur, and zinc, scrap tires can also contaminate the soil [31]. Scrap tires are not easily biodegradable in landfills. The volume that they occupy is also a major problem in landfills [32].

Instead of landfilling, recycling scrap tires have its own economic advantage. Scrap tires can be used as part of construction material due to their physical characteristics [33]. Ground scrap tires are used for roofing materials, sports tracks, and noise pollution barriers [32]. According to Dick et al. [34], pyrolysis is the most recommended method of recycling waste tires. The three valuable products of waste tires that are processed through pyrolysis are pyro-oil, pyro-gas, and pyro-char [35]. Due to its high carbon content, surface area, and porosity, pyro-char (activated carbon derived from the waste tire) can be used as an adsorbent for removing different pollutants from wastewater [24, 36–38].

Increasing the surface area of the activated carbon, which is derived from scrap tires, is the major problem that is faced during the preparation process [24]. Demineralization enhances the adsorption capacity of the adsorbent by removing inorganic minerals from the given adsorbent through a process called leaching [39]. This process increases the availability of the pours by removing the impurities (inorganic minerals) that blocked the pour structure, which in turn increases the surface area, micro, and mesopore volume [39]. Some of the inorganic minerals that are found in waste tires are iron, silicon dioxide, zinc, calcium, potassium, magnesium, chromium, manganese, sodium, nickel, and lead [40]. Moreover, demineralization lowers the ash content and increases the yield of the activated carbon [41]. Response surface methodology is one of the most efficient methods that is used to study and optimize experimental variables [42, 43]. It is used to study and optimize experimental variables. This methodology has an advantage in terms of evaluating the controlling effect of each parameter and their interaction by reducing the number of experiments [44].

Previously, research has been studied regarding the use of activated carbon derived from scrap tires for the removal of methylene blue dye from wastewater [2, 38, 45]. However, it is noted that no research is carried out regarding the synthesis optimization of activated carbon derived from scrap tires under response surface methodology. Teng et al. [46] studied the effect of impregnation ratio, pyrolysis temperature, and holding time on surface area and yield of activated carbon derived from scrap tires. However, it is noted that no research is carried out regarding the demineralization of activated carbon derived from scrap tires using $NaOH + H_2SO_4$ (1 : 1) as a demineralizing solvent for surface area enhancement. Therefore, this study aimed to optimize the synthesis of activated carbon driven from scrap tires in terms of yield and methylene blue removal.

2. Materials and Methods

2.1. Pretreatment of Scrap Tire. The scrap tires were collected from a local market, which is located in Addis Ketema subcity, Addis Ababa, Ethiopia. These tires were washed several times with detergent and tap water to remove dirt and dried at an ambient temperature 25±1°C. The cleaned tires were then cut into small pieces by sharp knives. The size of the

tires was further decreased by a high-speed multifunction miller (Model HC-700) and sieved to a size of 0.2 mm. The scrap tires were then washed several times with distilled water and dried in an oven (Model BOV-T50F) for 5 h at 60°C [47, 48].

2.2. Aqueous Solution Preparation. An aqueous solution of 1 g/L was prepared by adding 1g of methylene blue ($C_{16}H_{18}N_3SCl$, molecular weight: 319.85 g/mol) in a 1 L volumetric flask. Then, distilled water was filled to the mark of 1 L, and dissolution is performed using a magnetic stirrer. By using the concept of the dilution process, a different working solution was prepared.

2.3. Scrap Tire-Driven Activated Carbon (STAC) Synthesis Optimization. The chemical activation process was conducted in the presence of ethanol as a solvent. Thirty grams of the pretreated scrap tire sample was impregnated with KOH at various impregnation ratios (0–2 g/g) and impregnation time (12–36 hr). The impregnated sample was dried in an oven at 105°C. The sample was then pyrolyzed in a muffle furnace (Model Naberthrem F 330) in an inert environment, which is created by N_2 gas. Pyrolysis was carried out at different carbonization temperatures (700–900°C) for 2 hr [49]. After the activated sample was cooled, it was washed with 0.1 N HCl in 150 ml solution for 30 min. Then, the activated sample was washed several times with distilled water until the pH of the supernatant is 7. The activated sample was then dried in an oven at 105°C for 24 hr.

The synthesis process of the activated carbon was optimized by central composite design (CCD) using Minitab software Version 20.1.3 under response surface methodology (RSM). Impregnation ratio, impregnation time, and carbonization temperature were factors. These factors were fixed based on literature values. SCAC Yield and methylene blue (MB) removal efficiency were response variables.

According to the RSM of CCD, 20 experiments were conducted at different combinations of the three variables. The number of experiments was calculated using.

$$N = 2^F + 2\mathrm{F} + \mathrm{x0}, \tag{1}$$

where N is the number of experimental runs, F represents the factor number, and xo is the number of replicates at the central point. In this study, N is 20, F is 3 and xo is 6.

Of the 20 experiments, 5 experiments were replicated at center points to evaluate the error. Based on a set of experiments, the range of the variables, step size, and the central value were chosen as shown in Table 1.

The center points are used to determine the experimental error and the reproducibility of the data. The axial points are located at $(\pm\alpha, 0, 0)$, $(0, \pm\alpha, 0)$, and $(0, 0, \alpha)$. $\alpha = 1.0$ (face-centered) is the distance of the axial point from the center and makes the design rotatable. The experimental sequence was randomized to minimize the effect of the uncontrolled factor.

The experimental results were fitted using a polynomial quadratic equation to correlate the response variables. The general form of the polynomial quadratic equation shown in equation (2) was used to develop a model that predicts (estimates) the STAC yield and MB removal percentage at the designed variable combination. The model is also used to predict the individual and interaction effects of different parameters.

Table 1: Selected optimization variables.

Variables (factors)	Code	Coded variable levels		
		−1	0	1
Carbonization temperature (°C)	T	700	800	900
Impregnation ratio (g/g)	IR	0	1	2
Impregnation time (hrs.)	IT	12	24	36

$$R = \beta o + \sum_{i=1}^{k} \beta i x i + \sum_{i=1}^{k} \beta i i (x i)^2 + \sum_{i=1}^{k-1} \sum_{j=i+1}^{k} \beta i j x i x j \varepsilon, \tag{2}$$

where, R = predicted response, $\beta 0$ = constant coefficient, βi = linear effect coefficients, βii = quadratic effect coefficients, βiij = interaction effect coefficients, xi = independent variables.

The STAC yield was calculated by equation (3).

$$\text{Yield} = \frac{W_{ac}}{W_o} * 100, \tag{3}$$

where: W_o (g) is dry weight of the pretreated scrap tire and W_{ac} (g) is the dry weight of produced STAC.

To determine MB removal, 200 ml of 20 solutions, which have the same value of pH and initial MB concentration, were prepared in a 250 ml Erlenmeyer flask. The pH, initial concentration, adsorbent dose, and contact time were taken constant for all experiments at 9, 20 mg/L, 0.5 g, and 45 min, respectively [50]. The adsorption experiment was conducted at room temperature and at a mixing speed of 125 rpm [3]. The adsorbent was separated from the solution using Whatman filter paper 42. The final MB concentration was determined using a UV-visible spectrophotometer (JASCO V-770) at a wavelength of 668 nm [6].

MB removal efficiency was calculated by equation (4).

$$Re = \left(\frac{\mathrm{Co} - \mathrm{Ce}}{\mathrm{Co}}\right) * 100, \tag{4}$$

where: Re (%) is removal efficiency, Co (mg L^{-1}) is the initial concentration of MB, and Ce (mg L^{-1}) is the final MB concentration.

The optimized STAC is used in characterization, demineralization, isotherm, and kinetics study.

2.4. Characterization of the Activated Carbon. The moisture content (MC), volatile matter (VM), ash content (AC), and fixed carbon (FC) of the optimized STAC were determined according to ASTM standards (D 2866–2869) [18]. The bulk density of the STAC was determined by the water displacement method.

SEM (Model FEI Inspect F50) was used to determine the surface morphology of the pretreated sample, before activation and after adsorption. Standard procedures were followed in preparing the sample and operating the equipment [51, 52].

XRD (Model Olympus BTXH) was used at a diffraction angle of 2ø from 10 to 80° to determine the crystalline and amorphous nature of the sample after activation and after adsorption. The XRD was operated at 15 mA and a scanning rate of 4.2°C/min. The results were analyzed using origin software Version 9.55 [18].

BET surface area analyzer (Horiba, SA-9600) was used to determine the surface area of optimized STAC. The sample was analyzed by taking 0.4 g of STAC in three vacuum tubes for 2 h at 100°C [53].

2.5. Demineralization. The optimized STAC was demineralized for enhancing the surface area. The demineralization process was conducted using a solvent that is prepared by 5M NaOH + 98% H_2SO_4 (1 : 1). 20 g of optimized STAC followed by 1 L distilled water was added to 16 ml of the demineralization solvent in Erlenmeyer flask. The mixture was mixed using a hot plate stirrer (Model P40-HS) at a temperature, mixing speed, and mixing time of 100°C, 400 rpm, and 3 hr, respectively. Then the demineralized STAC was separated from the solution using Whatman filter paper 42. The separated demineralized STAC was then washed thoroughly with distilled water and dried in an oven at 110°C for 24 hr [39, 54]. The surface area of the demineralized STAC was analyzed by BET method.

2.6. Adsorption Isotherm. The adsorption isotherm was studied at room temperature by preparing 200 mL of different initial MB concentrations (100, 120, 140, 150, 170, and 190 mg/L) in a 250 mL Erlenmeyer flask [3]. The pH, adsorbent dose, contact time, and mixing speed were taken constant at 9, 0.5 g, 45 min, and 125 rpm, respectively.

Langmuir adsorption isotherm assumes monolayer adsorption of adsorbate on the adsorbent surface and adsorption energy is fixed at all points [55]. The linearized form of Langmuir isotherm model is shown in equation (5).

$$\frac{C_e}{q_e} = \frac{1}{q_m K_l} + \frac{C_e}{q_m}, \tag{5}$$

$$qe = \frac{co - ce}{m} \times v, \tag{6}$$

where q_e and q_m are the adsorbed amount at equilibrium and Langmuir maximum adsorption, respectively (mg g^{-1}), K_l is the constants of Langmuir (L mg^{-1}), V is the adsorbate volume (L), and m is the mass of adsorbent (g).

R_L is a dimensionless factor that predicts the appropriateness of the adsorption by the constants obtained from the Langmuir model and calculated using R_L.

$$R_L = \frac{1}{1 + Kl\, C_o}. \tag{7}$$

If $R_L > 1$, the used adsorbent is not appropriate for the adsorption of the adsorbate. If $R_L = 0$, adsorption on the adsorbent will be reversed. If $R_L = 1$, the isotherm is of linear type, and if $0 < R_L < 1$, the utilized adsorbent is appropriate.

Freundlich isotherm assumes a heterogeneous adsorption process [56]. The linearized form of Freundlich isotherm model is shown in equation (8).

$$\log q_e = \log K_f + \frac{1}{n} \log C_e, \tag{8}$$

where: q_e is the Equilibrium loading (mg g^{-1}), C_e is the Equilibrium concentration (mg L^{-1}), K_f is adsorption capacity ((mg g^{-1}) (L $mg^{-1})^{1/n}$), and n is the adsorption intensity. The value of the Freundlich constant (n) should lie in the range of 1–10 for favorable adsorption, the higher n value the better the adsorption.

Temkin adsorption isotherm assumes that the heat of adsorption for all molecules decreases with the coverage of the adsorbent surface [57, 58]. According to Togue Kamga [59], this model is only valid for a range of intermediate ion concentrations. The linearized form of Temkin adsorption isotherm is given by

$$qe = \left(\left(\frac{Rt}{b}\right) lnKT + \left(\frac{RT}{b}\right) lnCe\right), \tag{9}$$

where: b is Temkin constant which is related to the heat of sorption (J mol^{-1}) and KT is Temkin isotherm constant (L g^{-1}).

Dubinin-Radushkevich isotherm is an empirical isotherm model that expresses the distribution of Gaussian energy onto heterogeneous surfaces with an adsorption mechanism [44]. Since this model does not predict Henry's law at low temperatures, it is only suitable for an intermediate range of adsorbate concentration [60]. According to Boubaker et al. [44], the model states that the adsorption potential is variable and the free adsorption enthalpy was related to the degree of pores filling. This model determines whether the pollutant uptake mechanism is physical or chemical [42, 61]. The linearized form of Dubinin-Radushkevich isotherm adsorption isotherm is given by equation (10).

$$lnqe = lnqDR\max - \beta\epsilon^2, \tag{10}$$

$$\epsilon = R * T * \ln\left(1 + \left(\frac{1}{Ce}\right)\right), \tag{11}$$

where: lnqDRmax is the maximum adsorption capacity of Dubinin-Radushkevich isotherm (mg g^{-1}), β is Dubinin-Radushkevich constant ($mol^2\ kJ^{-2}$), ϵ is Polanyi potential, R is universal gas constant (8.31 $Jmol^{-1}\ K^{-1}$), and T is absolute temperature (K).

2.7. Adsorption Kinetics and Intraparticle Diffusion. The adsorption kinetics and intraparticle diffusion were studied in 200 ml solution at a fixed value of pH 9, adsorbent dose of 0.5 g, and mixing speed of 125 rpm. The experiments were carried out at room temperature and at different contact times (25, 50, 100, 200, 250, and 300 min) in a 250 mL Erlenmeyer flask [62]. In the solid-solution interface, the adsorbate removal rate is expressed by adsorption kinetics. The experimental data were fitted on pseudo-first-order and pseudo-second-order adsorption kinetics models [63]. The

integral form of pseudo-first-order and pseudo-second-order equations are expressed in equations (12) and (13), respectively.

$$\log\left(q - q_t\right) = \log q_e - \frac{K_1 t}{2.303}, \quad (12)$$

$$\frac{t}{q_t} = \frac{1}{K_2 q_e^2} + \frac{t}{q_e}, \quad (13)$$

$$qt = \frac{co - ct}{m} \times v, \quad (14)$$

where qe and qt (both in mg g^{-1}) are the amounts of MB adsorbed at equilibrium and at time t, respectively; $K1$ (min^{-1}) is the rate constant of pseudo-first-order; $K2$ (g mg^{-1} min^{-1}) is the rate constant of pseudo-second-order, V (L) is the volume of the solution, m (g) is the mass of adsorbent, and t (min) is contact time.

Weber-Morris intraparticle diffusion model was used to study the diffusion mechanism of MB [63]. The model equation is expressed in equation (16).

$$qt = k_{id} * t^{0.5} + c, \quad (15)$$

where k_{id} (mg. $g^{-1}min^{0.5}$) is the intraparticle diffusion rate constant and c is a constant number.

3. Results and Discussion

3.1. Synthesis Optimization of Activated Carbon. The synthesis of STAC was optimized by using the impregnation ratio (IR), impregnation time (IT), and carbonization temperatures (T) as a factor. STAC yield and MB removal efficiency were response variables as shown in Table 2.

The maximum STAC yield (68.35%) was obtained at an impregnation ratio of 2 g/g, impregnation time of 12 hr, and carbonization temperature of 700°C. The MB removal efficiency at these factors was 89.96%. The maximum MB removal efficiency (90.48%) was obtained at impregnation ratio, impregnation time, and carbonization temperature of 0 g/g, 12 hr, and 900°C, respectively. The STAC yield at these factors was 45.33%. The minimum STAC yield (34.03%) was obtained at impregnation ratio, impregnation time, and carbonization temperature of 0 g/g, 36 hr, and 900°C, respectively. The minimum MB removal efficiency (89.18%) was obtained at impregnation ratio, impregnation time, and carbonization temperature of 2 g/g, 36 hr, and 800°C, respectively.

The factor values that give relatively both maximum STAC yield and MB removal are considered optimum factor values that are used to synthesize STAC. Therefore, an impregnation ratio of 2 g/g, impregnation time of 12 hr, and carbonization temperature of 700 C was taken as optimum factor values for synthesizing STAC. According to Teng et al. [46], a higher value of yield is obtained at carbonization temperature, impregnation ratio, and carbonization time of 500 C, 4, and 1 hr, respectively. Moreover, the maximum value of BET surface area was obtained at a carbonization temperature of 700 C, impregnation ratio of 4, and carbonization time of 1 hr. The maximum MB removal efficiency was compared with previous studies as shown in Table 3.

Table 2: Optimization of STAC synthesis.

IR (g/g)	IT (hr.)	T (C°)	Yield (%)	MB removal (%)
1	24	900	39.98	90.23
0	24	900	34.03	90.21
1	24	700	49.91	89.92
0	12	900	45.56	89.85
1	12	700	54.66	89.56
0	12	900	45.33	90.48
1	24	800	46.68	89.47
0	36	900	44.66	90.46
2	36	800	59.19	89.18
2	12	700	68.35	89.96
1	36	800	52.31	89.41
0	24	800	43.66	89.79
1	24	800	46.67	89.51
1	24	800	43.68	89.53
2	24	800	49.24	89.48
1	24	800	43.69	89.55
1	24	800	48.69	89.58
2	12	700	35.33	90.25
1	36	800	49.67	89.63
2	36	700	38.66	90.31

The effect of carbonization temperature, impregnation time, and impregnation ratio on STAC yield and MB removal is presented in Figure 1.

As shown in Figures 1(a)–1(c), the STAC yield decreases with the increment of carbonization temperature. This might be due to a higher degradation of rubber and other tire components at an enhanced temperature, which results in loss of weight [72]. STAC yield decreased with the increment of Impregnation time. This might be due to the collapse of pores and a decrease in surface area [73]. Increasing the impregnation ratio has facilitated the increment of the yield due to the addition of extra mass to the precursor [74].

As shown in Figures 1(d)–1(f), MB removal decreased as carbonization temperature increased. This might be due to the collapse of pores and carbon matrix at high temperatures [75]. MB removal increased with the increment of impregnation ratio. This might be due to the increment of surface area by chemical activation [46]. As the impregnation time increased, the MB removal efficiency decreased continuously. This might be due to the shrinkage of char structure, widening and combining of some micropores into mesopores, which decreased the adsorption capability of the adsorbent [73].

Due to the sorption capacity and pore structure of the activated carbon, the MB molecules can be adsorbed on the surface of the adsorbent [76]. According to Gao et al. [77], the presence of the micropores present in the activated carbon and the attraction of the Vander Waals forces are the main adsorption mechanisms of pollutants.

3.2. ANOVA and Development of Regression Model Equation. The regression coefficient for STAC yield ($R^2 = 0.957$) and MB removal ($R^2 = 0.992$) indicates that the quadratic regression model best fits the experimental data for both

Table 3: Comparison of MB removal efficiency of STAC with other researches.

Adsorbent	Removal efficiency (%)	Reference
STAC	90.48	This study
Ficus carica bast	85.00	Pathania et al. [64]
Eucalyptus leaves	86.66	Ghosh et al. [65]
Jackfruit leaf powder	85.00	Ahmed et al. [66]
Black tea wastes	75.00	Ullah et al. [67]
TiO_2/montmorillonite-albumin nanocomposite	84.45	Varmazyar et al. [68]
Parthenium hysterophorus	94.00	Fito et al. [3]
Corn husk	97.30	Khodaie et al. [69]
Rice husk biochar	98.90	Ahmad et al. [70]
Cotton stem biochar	96.28	Wang and Liu [71]

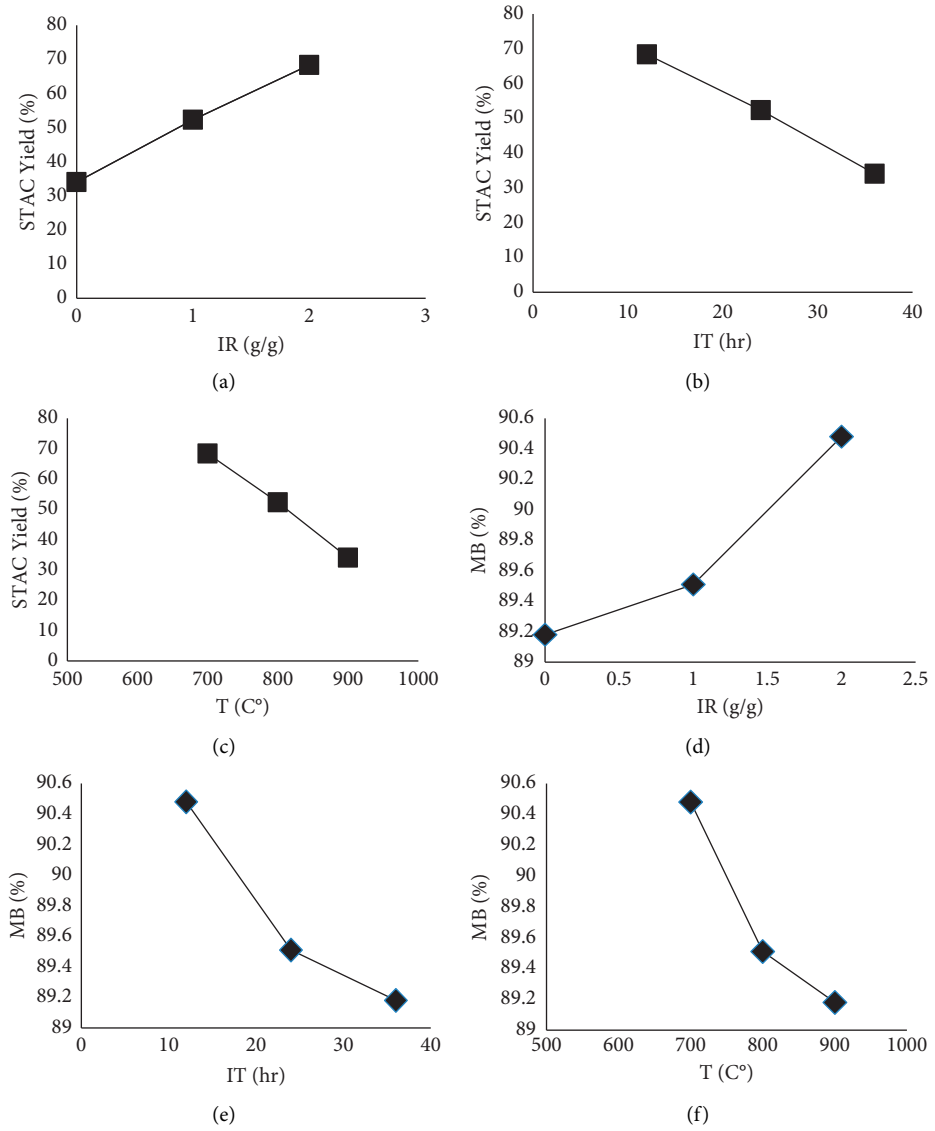

Figure 1: Effect of individual factors on STAC yield (a–c) and MB removal (d–f).

response variables. The Predicted R^2 value of the STAC yield is 0.872, which is in reasonable agreement with the adjusted R^2 value of 0.919. For MB removal, the predicted R^2 value is 0.972 and the adjusted R^2 value is 0.984. This indicates that the predicted and adjusted value is in satisfactory agreement.

The implication and suitability of the models for both STAC yield and MB removal were also tested by analysis of variance (ANOVA) as shown in Table 4. The mean squares were calculated by dividing the sum of the squares of each of the various sources and the mode and the error variance were calculated by the respective degrees of freedom. The *F*-value is the ratio of the

Table 4: Response surface quadratic model of ANOVA for MB removal.

Source	STAC yield					MB removal				
	d*f*	Sum of squares	Mean square	*F*-value	*P* value	d*f*	Sum of squares	Mean square	*F*-value	*P* value
Model	9	1131.76	125.751	25.18	0.001	9	2.82914	0.314348	137.97	0.001
T-carbonization temperature	1	382.91	382.913	76.68	0.001	1	0.13225	0.132250	58.05	0.001
IT-impregnation time	1	41.53	41.534	8.32	0.016	1	0.02809	0.028090	12.33	0.006
IR-impregnation ratio	1	79.92	79.919	16.00	0.003	1	0.32761	0.327610	143.79	0.001
T^2	1	34.76	34.763	6.96	0.025	1	0.75404	0.754036	330.96	0.001
IT^2	1	68.33	68.326	13.68	0.004	1	0.01211	0.012111	5.32	0.044
IR^2	1	11.56	11.562	2.32	0.159	1	0.01924	0.019236	8.44	0.016
T ∗ IT	1	23.22	23.222	4.65	0.056	1	0.28880	0.288800	126.76	0.056
T ∗ IR	1	518.58	518.581	103.85	0.001	1	0.40500	0.405000	177.76	0.001
IT ∗ IR	1	1.04	1.044	0.21	0.657	1	0.19845	0.198450	87.10	0.001
Lack-of-fit	5	19.18	3.836	0.62	0.691	5	0.00723	0.001447	0.4e	0.790
Pure error	5	30.75	6.151			5	0.01555	0.003110		
Total	19	1181.69				19	2.85192			

mean square contributing to regression to the mean square contributing to error. The greater the *F*-value, the more is the significance of the corresponding variable to cause an effect.

As shown in Table 4, the model *F*-value of 25.18 for STAC yield and 137.97 for MB removal implies that this model was significant. The lack of fit *F*-value of 0.62 for STAC yield and 0.47 for MB removal implies that the lack of fit is not significant relative to the pure error. The significance of the model is also tested by *P* value. If the *P* values of the model terms are less than 0.05, they are statistically significant. The ANOVA of the quadratic model for STAC yield indicates that T, IT, IR, T^2, IT^2, and T ∗ IR are statistically significant ($P < 0.05$) but IR^2, T ∗ IT, and IT ∗ IR are not statistically significant ($P > 0.05$). For MB removal, the model indicates that T, IT, IR, T^2, IT^2 and T ∗ IR, IR^2, and IT ∗ IR are statistically significant ($P < 0.05$) but T ∗ IT is not statistically significant ($P < 0.05$). The regression model equation was developed by removing the insignificant model terms. The model equation that is developed by three factors or twenty experiments for STAC yield and MB removal is described in equations (16) and (17), respectively.

$$\begin{aligned}\text{Yield}(\%) &= -149.5 + 0.553\text{T} - 2.937\text{IT} + 72.06\text{IR} \\ &\quad - 0.000356T^2 + 0.03461\,\text{IT}^2 - 0.08051T * IR,\end{aligned} \tag{16}$$

$$\begin{aligned}\text{MBR}(\%) &= 126.77 - 0.08868\text{T} - 0.0958\text{IT} - 1.833\text{IR} \\ &\quad + 0.000052T^2 - 0.000461IT^2 + 0.0836\text{IR}^2 \\ &\quad + 0.002250\text{T} * \text{IR} - 0.01312\text{IT} * \text{IR},\end{aligned} \tag{17}$$

where: T is Carbonization temperature, IR is Impregnation ratio, IT is Impregnation time, T ∗ IR is the interaction effect of time and impregnation ratio, IT ∗ IR is the interaction effect of impregnation time and impregnation ratio, MBR is Methylene blue removal (%) and Y is STAC yield (%).

3.3. The Interaction Effect of Factors on STAC Yield and MB Removal. Out of the three interaction effects, only one interaction (T ∗ IR) is statistically significant ($P < 0.05$) for STAC yield and two interactions (T ∗ IR and IT ∗ IR) are statistically significant ($P < 0.05$) for MB removal as shown in Table 4. The three-dimensional response surface plot of the statistically significant ($P < 0.05$) interaction effects on STAC yield and MB removal is presented in Figure 2.

3.4. Characteristics of Optimized Activated Carbon

3.4.1. Proximate Analysis. The MC, VM, AC, FC, and bulk density of the STAC were 6.13%, 9.42%, 5.34%, 79.11%, and 0.89 mg/L, respectively. The low value of MC, VM, AC, and the higher value of FC indicates that the STAC has a good adsorbent characteristic [78].

3.4.2. Scanning Electron Microscope (SEM). The surface morphology of scrap tires before activation (raw), after activation, and after adsorption are presented in Figure 3. In all three SEM micrograph images, a magnification of 10 μm was used. Compared to the raw scrap tire, the activated scrap tire shows a highly porous morphological structure with heterogeneous, irregular, and small pores of various shapes and sizes. The internal structure of the STAC was irregular with many gullies and openings. This might be due to the chemical and thermal activation of the scrap tire [53]. After adsorption, the number of pours decreased. This might be due to the adsorption of MB on the internal and external pore structure of the STAC [79].

3.4.3. X-Ray Diffraction (XRD). The X-ray diffraction of scrap tires after activation and after adsorption is presented in Figure 4. The large hill of A, from $2\theta = 19.56^\circ$ to 36.56° corresponding to side spacing 4.5347 Å to 2.4558 Å indicated the existence of amorphous carbon together with other crystalline compounds. These crystalline compounds were found to be ZnO (zincite) and β-ZnS (wurtzite). Similar results were reported by Ilnicka et al. [80]; López et al. [81]; Undri et al. [82]. ZnO (zincite) is the major component of the scrap tire. However, according to Amirza et al. [83],

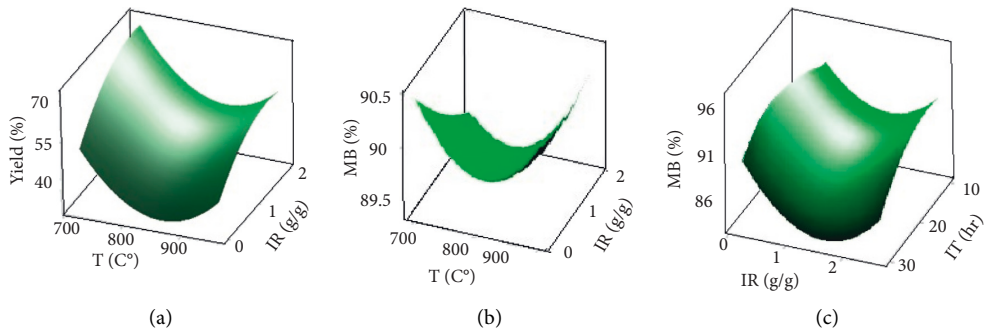

(a) (b) (c)

Figure 2: 3D plot of statistically significant interactions (the interaction effect of T and IR on STAC yield (a); T and IR on MB removal (b); and IR and IT on MB removal (c)).

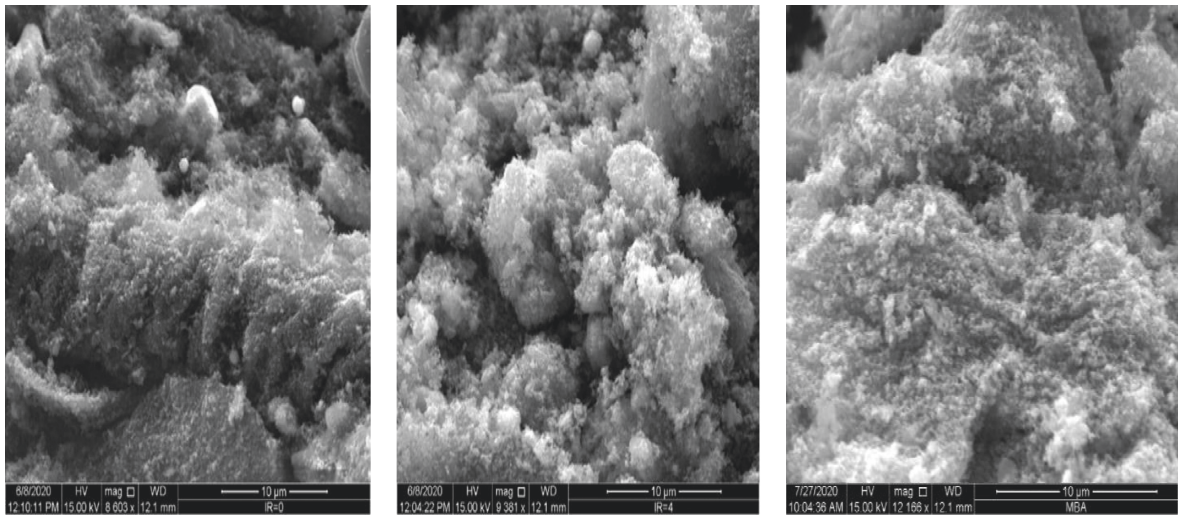

(a) (b) (c)

Figure 3: SEM image scrap tire for raw (a), after activation (b), and after adsorption (c).

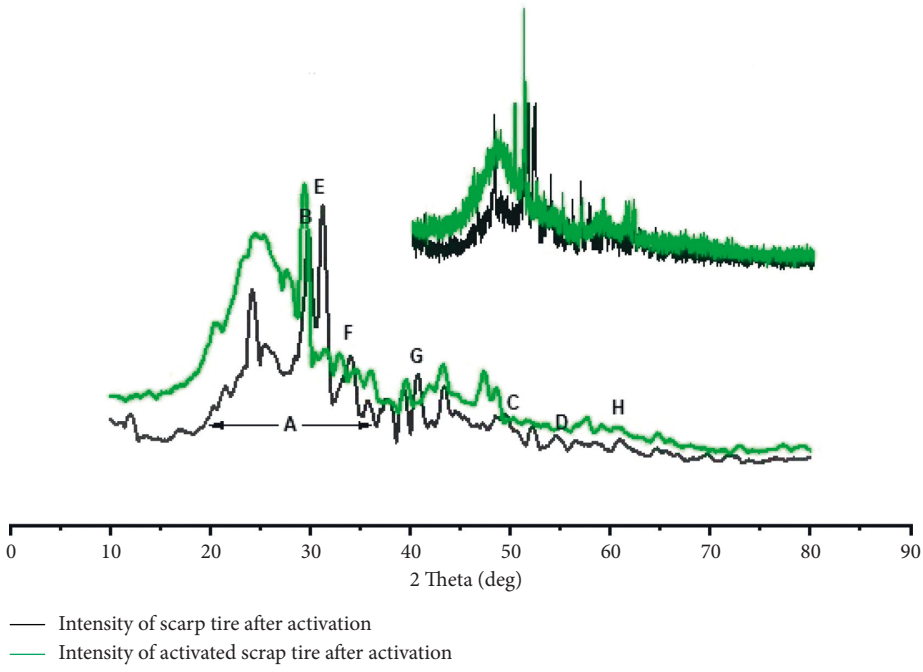

Figure 4: XRD analysis of scrap tire after activation (black color) and after adsorption (green color).

Table 5: Adsorption isotherm.

Isotherm model		Optimized	Demineralized
Langmuir	R^2	0.957	0.946
	q_m (mg g^{-1})	73.53	92.59
	K_l (L mg^{-1})	0.130	0.1314
	Equation	$Y = 0.0136X + 0.1043$	$Y = 0.0108X + 0.0822$
Freundlich	R^2	0.956	0.965
	N	1.675	1.5731
	K_f ((mg g^{-1}) (L $mg^{-1})^{1/n}$)	10.277	14.692
	Equation	$Y = 0.5967X + 1.0119$	$Y = 0.6357X + 1.1671$
Temkin	R^2	0.974	0.982
	b (J mol^{-1})	16.427	19.862
	K_T (L g^{-1})	1.265	1.834
	Equation	$Y = 16.43X + 3.89$	$Y = 19.86X + 12.05$
Dubinin-Radushkevich	R^2	0.972	0.947
	qDRmax (mg g^{-1})	99.48	134.29
	β (mol^2 kJ^{-2})	$1 * 10^{-6}$	$2 * 10^{-6}$
	Equation	$Y = -1 * 10^{-6}X + 4.60$	$Y = -2 * 10^{-6}X + 4.90$

Table 6: Adsorption kinetics and intraparticle diffusion.

Kinetics model		Optimized	Demineralized
Pseudo-first-order	R^2	0.987	0.842
	q_e (mg g^{-1})	0.016	0.001
	K_1 (min^{-1})	−0.051	−0.017
	Equation	$Y = 0.024X - 1.85$	$Y = 0.042X - 3.20$
Pseudo-second-order	R^2	0.996	0.999
	q_e (mg g^{-1})	11.166	12.976
	K_2 (g mg^{-1} min^{-1})	−0.027	−0.397
	Equation	$Y = 13.659X - 3.0697$	$Y = 12.715X + 0.0931$
Intraparticle diffusion	R^2	0.912	0.898
	C	13.017	13.679
	K_{ID} (mg $g^{-1}min^{0.5}$)	−0.105	−0.105
	Equation	$Y = -0.105X + 13.017$	$Y = -0.105X + 13.679$

while carbonization, the ZnO reacted with sulfur compounds existing in the furnace, creating zinc sulfide in the crystalline form of β-ZnS (wurtzite). Ali and Alrafai [84] also reported the conversion of ZnO into ZnS due to desulfurization reaction and the volatilization process.

The peaks labeled as B, C, and D at peak positions of $2\theta = 29.76^\circ$, 49.58°, and 54.56° corresponding to side spacing 2.9996 Å, 1.8371 Å, and 1.6806 Å showed the presence of ZnS. Different peaks labeled at E, F, G, and H with different peak positions of $2\theta = 31.34^\circ$, 34.1 , 40.86 , and 47.3 , corresponding to side spacing 2.8519 Å, 2.6271 Å, 2.2067 Å, and 1.9202 Å, respectively. The presence of crystalline structure is indicated by these high-intensity peaks [85]. On the other hand, similar peaks were observed by MB adsorbed STAC samples, with the exception of increased intensity and full width half maximum (FWHM) values. As 2θ values increased in the spectra pattern, the peak intensity decreased, which indicates the presence of an amorphous carbon arrangement [18].

3.5. Surface Area Study of Optimized and Demineralized Activated Carbon. A demineralization experiment was conducted to enhance the surface area of the optimized STAC. In this study, inorganic minerals such as ZnO were removed from the pores and polymeric resins of rubber, which could lead to enhancement of the surface area. The surface area of optimized STAC was 54.93 m^2/g. A surface area of 88 m^2/g was reported by Jankovská et al. [86] for activated carbon driven from scrap tires. The surface area of optimized STAC that is demineralized by $NaOH + H_2SO_4$ was 260.26 m^2/g. This indicates that the surface area of optimized STAC increased due to the demineralization process [39]. A higher surface area value of 493 m^2/g was reported by Ali et al. [24] for activated carbon derived from scrap tires.

3.6. Adsorption Mechanism

3.6.1. Adsorption Isotherm. Langmuir, Freundlich, Temkin, and Dubinin-Radushkevich adsorption isotherm models were used to study the adsorption mechanism. Regression coefficient (R^2) was used to indicate the isotherm model that best fits with experimental data. For both optimized and demineralized STAC, Temkin adsorption isotherm model with R^2 values of 0.974 and 0.982 best describes the adsorption mechanism as shown in Table 5. This indicates that the heat of adsorption of all molecules in the layer reduces linearly [87]. This results from the increase of surface

coverage [57]. Temkin adsorption isotherm also indicates that up to maximum binding energy, the adsorption is characterized by a uniform distribution of binding energies [61, 88].

3.6.2. Adsorption Kinetics and Intraparticle Diffusion. The adsorption kinetics of the adsorption process was examined by pseudo-first-order and pseudo-second-order models. For both optimized and demineralized STAC, pseudo-second-order adsorption kinetics model with R^2 values of 0.996, and 0.999 best fits with the experimental data as shown in Table 6. This indicates that the adsorption process is controlled by chemical reactions [89]. The diffusion mechanism was studied by the intraparticle diffusion model. From the linear regression equation, it can be noted that values of C of both the optimized and demineralized STAC are not equal to zero. This indicates that intraparticle diffusion was not the only rate-controlling step [90].

4. Conclusion

The STAC synthesis was optimized using central composite design under response surface methodology. Impregnation ratio of 2 g/g, impregnation time of 12 hr, and carbonization temperature of 700°C was taken as optimum factor values for synthesizing STAC. The regression coefficient for STAC yield and MB removal with R^2 values of 0.957 and 0.992 indicates that the quadratic regression model best fits the experimental data for both response variables. From ANOVA, it can be noted that the interaction effect of carbonization temperature and impregnation ratio on STAC yield is the only significant ($P < 0.05$) interaction. Moreover, for MB removal, the interaction effect of carbonization temperature and impregnation ratio and the interaction effect of impregnation time and impregnation ratio is the only significant ($P < 0.05$) interactions. The proximate analysis indicates that the STAC has a good adsorbent characteristic. The surface area of optimized STAC was enhanced from 54.93 m^2/g to 260.26 m^2/g by the demineralization process using $NaOH + H_2SO_4$ at (1 : 1) as a solvent. Temkin adsorption isotherm with R^2 values of 0.974 and 0.982 best fits with the experimental data for both optimized and demineralized STAC respectively. This indicates that the heat of adsorption of all molecules in the layer reduces linearly with coverage. For both optimized and demineralized STAC, pseudo-second-order adsorption kinetics with R^2 value of 0.996 and 0.999 best fits the experimental data, respectively. This indicates that the adsorption process is controlled by chemical reactions. From the intraparticle diffusion model, it can be noted that intraparticle diffusion was not the only rate-controlling step for both optimized and demineralized STAC. Generally, it can be concluded that the optimized STAC that is demineralized by $NaOH + H_2SO_4$ solvent has a promising potential to be used as a low-cost adsorbent in developing countries including Ethiopia. However, further investigation needs to be conducted before scaling up at the industrial level.

Data Availability

All the data used to support the findings of this study are included in the article.

Conflicts of Interest

The authors declare that they have no conflicts of interest.

Acknowledgments

This study was financially supported by Addis Ababa Science and Technology University.

References

[1] T.-C. Lee, S. Wang, Z. Huang et al., "Tea stem as a sorbent for removal of methylene blue from aqueous phase," *Advances in Materials Science and Engineering*, vol. 2019, Article ID 9723763, 15 pages, 2019.

[2] M. S. H. Shaid, M. A. Ahmad Zaini, and N. S. Nasri, "Isotherm studies of methylene blue adsorption onto waste tyre pyrolysis powder-based activated carbons," *Malaysian Journal of Fundamental and Applied Sciences*, vol. 13, no. 4, pp. 671–675, 2017.

[3] J. Fito, S. Abrham, and K. Angassa, "Adsorption of methylene blue from textile industrial wastewater onto activated carbon of Parthenium hysterophorus," *International Journal of Environmental Research*, vol. 14, no. 5, pp. 501–511, 2020.

[4] R. H. Khuluk, A. Rahmat, B Buhani, and S Suharso, "Removal of methylene blue by adsorption onto activated carbon from coconut shell (Cocous nucifera L.)," *Indonesian Journal of Science and Technology*, vol. 4, no. 2, pp. 229–240, 2019.

[5] Y. Kuang, X. Zhang, and S. Zhou, "Adsorption of methylene blue in water onto activated carbon by surfactant modification," *Water*, vol. 12, no. 2, p. 587, 2020.

[6] M. A. Al-Ghouti and R. S. Al-Absi, "Mechanistic understanding of the adsorption and thermodynamic aspects of cationic methylene blue dye onto cellulosic olive stones biomass from wastewater," *Scientific Reports*, vol. 10, no. 1, Article ID 15928, 2020.

[7] A. S. Al-Wasidi, I. I. S. AlZahrani, A. M. Naglah et al., "Effective removal of methylene blue from aqueous solution using metal-organic framework; modelling analysis, statistical physics treatment and DFT calculations," *ChemistrySelect*, vol. 6, no. 41, Article ID 11431, 2021.

[8] H. Md Anawar and R. Chowdhury, "Remediation of polluted river water by biological, chemical, ecological and engineering processes," *Sustainability*, vol. 12, no. 17, 2020.

[9] B. Lellis, C. Z. Fávaro-Polonio, J. A. Pamphile, and J. C. Polonio, "Effects of textile dyes on health and the environment and bioremediation potential of living organisms," *Biotechnology Research and Innovation*, vol. 3, no. 2, pp. 275–290, 2019.

[10] R. K. Patel, R. Prasad, R. Shankar, P. Khare, and M. Yadav, "Adsorptive removal of methylene blue dye from soapnut shell & pineapple waste derived activated carbon," *International Journal of Engineering, Science and Technology*, vol. 13, no. 1, pp. 81–87, 2021.

[11] T. A. Aragaw and F. M. Bogale, "Biomass-based adsorbents for removal of dyes from wastewater: a review," *Frontiers in Environmental Science*, vol. 9, 2021.

[12] N. Y. Donkadokula, A. K. Kola, I. Naz, and D. Saroj, "A review on advanced physico-chemical and biological textile dye wastewater treatment techniques," *Reviews in Environmental Science and Biotechnology*, vol. 19, no. 3, pp. 543–560, 2020.

[13] S. Dutta, B. Gupta, S. K. Srivastava, and A. K. Gupta, "Recent advances on the removal of dyes from wastewater using

various adsorbents: a critical review," *Materials Advances*, vol. 2, 2021.

[14] K. O. Iwuozor, J. O. Ighalo, E. C. Emenike, L. A. Ogunfowora, and C. A. Igwegbe, "Adsorption of methyl orange: a review on adsorbent performance," *Current Research in Green and Sustainable Chemistry*, vol. 4, Article ID 100179, 2021.

[15] O. J. Ajala, J. O. Tijani, M. T. Bankole, and A. S. Abdulkareem, "Wastewater treatment technologies," in *Inorganic-Organic Composites for Water and Wastewater Treatment*, E. Lichtfouse, S. S. Muthu, and A. Khadir, Eds., pp. 1–28, Springer Singapore, Singapore, 2022.

[16] P. P. Bhave and D. Yeleswarapu, "Removal of indoor air pollutants using activated carbon—a review," *Global Challenges in Energy and Environment*, vol. 1, pp. 65–75, 2020.

[17] E. E. Jasper, J. C. Onwuka, and Y. M. Bidam, "Screening of factors that influence the preparation of Dialium guineense pods active carbon for use in methylene blue adsorption: a full factorial experimental design," *Bulletin of the National Research Centre*, vol. 45, no. 1, p. 168, 2021.

[18] T. S. Tessema, A. T. Adugna, and M. Kamaraj, "Removal of Pb (II) from synthetic solution and paint industry wastewater using activated carbon derived from african arrowroot (canna indica) stem," *Advances in Materials Science and Engineering*, vol. 2020, 10 pages, 2020.

[19] J. Ali, E. M. Bakhsh, N. Hussain et al., "A new biosource for synthesis of activated carbon and its potential use for removal of methylene blue and eriochrome black T from aqueous solutions," *Industrial Crops and Products*, vol. 179, Article ID 114676, 2022.

[20] R. Remmani, R. Makhloufi, M. Miladi, A. Ouakouak, A. R. Canales, and D. Núñez-Gómez, "Development of low-cost activated carbon towards an eco-efficient removal of organic pollutants from oily wastewater," *Polish Journal of Environmental Studies*, vol. 30, no. 2, pp. 1801–1808, 2021.

[21] J. U. Ani, K. G. Akpomie, U. C. Okoro, L. E. Aneke, O. D. Onukwuli, and O. T. Ujam, "Potentials of activated carbon produced from biomass materials for sequestration of dyes, heavy metals, and crude oil components from aqueous environment," *Applied Water Science*, vol. 10, no. 2, p. 69, 2020.

[22] V. Balasubramanian, T. Daniel, J. Henry, G. Sivakumar, and K. Mohanraj, "Electrochemical performances of activated carbon prepared using eggshell waste," *SN Applied Sciences*, vol. 2, no. 1, p. 127, 2020.

[23] I. Bianco, D. Panepinto, and M. Zanetti, "End-of-Life tyres: comparative life cycle assessment of treatment scenarios," *Applied Sciences*, vol. 11, no. 8, 2021.

[24] U. F. M. Ali, F. Hussin, S. C. Gopinath et al., "Advancement in recycling waste tire activated carbon to potential adsorbents," *Environmental Engineering Research*, vol. 27, 2021.

[25] J. Araujo-Morera, R. Verdejo, M. A. López-Manchado, and M. Hernández Santana, "Sustainable mobility: the route of tires through the circular economy model," *Waste Management*, vol. 126, pp. 309–322, 2021.

[26] Y. Dong, Y. Zhao, M. U. Hossain, Y. He, and P. Liu, "Life cycle assessment of vehicle tires: a systematic review," *Cleaner Environmental Systems*, vol. 2, Article ID 100033, 2021.

[27] G. A. Alamrew, "A business opportunity study on recovery of fuel oil, carbon black and steel from used tyers (Executive Master of Business Administration)," 2014, http://213.55.95.56/bitstream/handle/123456789/13399/Gebru%20Ayehubzu.pdf?sequence=1&isAllowed=y.

[28] G. Przydatek, G. Budzik, and M. Janik, "Effectiveness of selected issues related to used tyre management in Poland," *Environmental Science and Pollution Research*, vol. 29, no. 21, Article ID 31467, 2022.

[29] S. Dabic-Miletic, V. Simic, and S. Karagoz, "End-of-life tire management: a critical review," *Environmental Science and Pollution Research*, vol. 28, no. 48, Article ID 68053, 2021.

[30] J. Downard, A. Singh, R. Bullard et al., "Uncontrolled combustion of shredded tires in a landfill–Part 1: characterization of gaseous and particulate emissions," *Atmospheric Environment*, vol. 104, pp. 195–204, 2015.

[31] A. Tasalloti, G. Chiaro, A. Murali, L. Banasiak, A. Palermo, and G. Granello, "Recycling of end-of-life tires (ELTs) for sustainable geotechnical applications: a New Zealand perspective," *Applied Sciences*, vol. 11, no. 17, 2021.

[32] A. Mohajerani, L. Burnett, J. V. Smith et al., "Recycling waste rubber tyres in construction materials and associated environmental considerations: a review," *Resources, Conservation and Recycling*, vol. 155, Article ID 104679, 2020.

[33] O. Y. Bayraktar, G. Saglam-Citoglu, and A. Abo Aisha, "The use of scrap tires in the construction sector," *International Journal of Trend in Research and Development*, vol. 6, no. 1, pp. 253–256, 2019.

[34] D. T. Dick, O. Agboola, and A. Ayeni, "Pyrolysis of waste tyre for high-quality fuel products: a review," *AIMS Energy*, vol. 8, no. 5, pp. 869–895, 2020.

[35] A. Alsaleh and M. L. Sattler, "Waste tire pyrolysis: influential parameters and product properties," *Current Sustainable/Renewable Energy Reports*, vol. 1, no. 4, pp. 129–135, 2014.

[36] K. Frikha, L. Limousy, J. Pons Claret et al., "Potential valorization of waste tires as activated carbon-based adsorbent for organic contaminants removal," *Materials*, vol. 15, no. 3, p. 1099, 2022.

[37] K. Manirajah, S. V. Sukumaran, N. Abdullah, H. A. Razak, and N. Ainirazali, "Evaluation of low cost-activated carbon produced from waste tyres pyrolysis for removal of 2-chlorophenol," *Bulletin of Chemical Reaction Engineering and Catalysis*, vol. 14, no. 2, p. 443, 2019.

[38] E. Elmaslar Özbaş, B. Balçık, and H. Ozcan, "Preparation of activated carbon from waste tires, and its use for dye removal," *Desalination and Water Treatment*, vol. 172, pp. 78–85, 2019.

[39] A. Bazan-Wozniak, P. Nowicki, and R. Pietrzak, "The effect of demineralization on the physicochemical and sorption properties of activated bio-carbons," *Adsorption*, vol. 25, no. 3, pp. 337–343, 2019.

[40] M. Selbes, O. Yilmaz, A. A. Khan, and T. Karanfil, "Leaching of DOC, DN, and inorganic constituents from scrap tires," *Chemosphere*, vol. 139, pp. 617–623, 2015.

[41] O. R. Ogunsakin, S. Holberg, X. Wang, A. Goroncy, J. Adams, and P. Johnson, "Acid demineralization effect on the sonication-assisted solvent extraction of vitrinite coal of the Powder River Basin," *Fuel*, vol. 308, Article ID 121989, 2022.

[42] S. Karoui, R. Ben Arfi, K. Mougin, A. Ghorbal, A. A. Assadi, and A. Amrane, "Synthesis of novel biocomposite powder for simultaneous removal of hazardous ciprofloxacin and methylene blue: central composite design, kinetic and isotherm studies using Brouers-Sotolongo family models," *Journal of Hazardous Materials*, vol. 387, Article ID 121675, 2020.

[43] S. Karoui, R. Ben Arfi, M. J. Fernández-Sanjurjo, A. Nuñez-Delgado, A. Ghorbal, and E. Álvarez-Rodríguez, "Optimization of synergistic biosorption of oxytetracycline and cadmium from binary mixtures on reed-based beads: modeling study using Brouers-Sotolongo models," *Environmental*

Science and Pollution Research, vol. 28, no. 34, Article ID 46431, 2021.

[44] H. Boubaker, R. Ben Arfi, K. Mougin et al., "New optimization approach for successive cationic and anionic dyes uptake using reed-based beads," *Journal of Cleaner Production*, vol. 307, Article ID 127218, 2021.

[45] H. Daraei and A. Mittal, "Investigation of adsorption performance of activated carbon prepared from waste tire for the removal of methylene blue dye from wastewater," *Desalination and Water Treatment*, vol. 90, pp. 294–298, 2017.

[46] H. Teng, Y.-C. Lin, and L.-Y. Hsu, "Production of activated carbons from pyrolysis of waste tires impregnated with potassium hydroxide," *Journal of the Air & Waste Management Association*, vol. 50, no. 11, pp. 1940–1946, 2000.

[47] A. Amenaghawon, F. Aisien, and O. Agho, "Adsorption of toluene by waste tyre rubber granules: effect of operating variables, kinetic and isotherm studies," *International Journal of Scientific Research in Knowledge*, vol. 1, no. 10, pp. 427–438, 2013.

[48] K. M. Dimpe, J. C. Ngila, and P. N. Nomngongo, "Application of waste tyre-based activated carbon for the removal of heavy metals in wastewater," *Cogent Engineering*, vol. 4, no. 1, Article ID 1330912, 2017.

[49] A. E. Kassa, N. T. Shibeshi, and B. Z. Tizazu, "Characterization and optimization of calcination process parameters for extraction of aluminum from Ethiopian kaolinite," *International Journal of Chemical Engineering*, vol. 2022, Article ID 5072635, 18 pages, 2022.

[50] E. Fadhil Nassar, D. Zageer, D. H Fadhil, and M. S Khlaf, "Elimination of methylene blue from solution using modified scrap tire," *Oriental Journal of Physical Sciences*, vol. 3, no. 1, pp. 62–67, 2018.

[51] D. Bedada, K. Angassa, A. Tiruneh, H. Kloos, and J. Fito, "Chromium removal from tannery wastewater through activated carbon produced from Parthenium hysterophorus weed," *Energy, Ecology and Environment*, vol. 5, no. 3, pp. 184–195, 2020.

[52] J. F. Nure, N. T. Shibeshi, S. L. Asfaw, W. Audenaert, and S. W. Hulle, "COD and colour removal from molasses spent wash using activated carbon produced from bagasse fly ash of Matahara sugar factory, Oromiya region, Ethiopia," *WaterSA*, vol. 43, no. 3, p. 470, 2017.

[53] A. Tebeje, Z. Worku, T. T. I. Nkambule, and J. Fito, "Adsorption of chemical oxygen demand from textile industrial wastewater through locally prepared bentonite adsorbent," *International journal of Environmental Science and Technology*, vol. 19, no. 3, pp. 1893–1906, 2021.

[54] F. López, T. Centeno, O. Rodríguez, and F. Alguacil, "Preparation and characterization of activated carbon from the char produced in the thermolysis of granulated scrap tyres," *Journal of the Air & Waste Management Association*, vol. 63, no. 5, pp. 534–544, 2013.

[55] K. N. S. Budhiary and I. Sumantri, "Langmuir and Freundlich isotherm adsorption using activated charcoal from banana peel to reduce total suspended solid (TSS) levels in tofu industry liquid waste," in *Proceedings of the IOP Conference Series: Materials Science and Engineering*, vol. 1053, 2021.

[56] C. Aggelopoulos, E. Moschopoulou, P. Klepetsanis, and C. Tsakiroglou, "Valorization of fruit wastes (pistachio shells) as adsorbent for the removal of Zn from aqueous solutions under adverse acidic conditions," *Desalination and Water Treatment*, vol. 74, pp. 174–183, 2017.

[57] N. Ayawei, A. N. Ebelegi, and D. Wankasi, "Modelling and interpretation of adsorption isotherms," *Journal of Chemistry*, vol. 2017, Article ID 3039817, 11 pages, 2017.

[58] F. Batool, J. Akbar, S. Iqbal, S. Noreen, and S. N. A. Bukhari, "Study of isothermal, kinetic, and thermodynamic parameters for adsorption of cadmium: an overview of linear and nonlinear approach and error analysis," *Bioinorganic Chemistry and Applications*, vol. 2018, 2018.

[59] F. Togue Kamga, "Modeling adsorption mechanism of paraquat onto Ayous (Triplochiton scleroxylon) wood sawdust," *Applied Water Science*, vol. 9, no. 1, 2019.

[60] T. Santhi, S. Manonmani, and T. Smitha, "Removal of malachite green from aqueous solution by activated carbon prepared from the epicarp of Ricinus communis by adsorption," *Journal of Hazardous Materials*, vol. 179, no. 1-3, pp. 178–186, 2010.

[61] R. Ben Arfi, S. Karoui, K. Mougin et al., "Enhanced Malachite Green uptake using chemically-modified reed-based powder: equilibrium, kinetics, mechanism, and reusability," *International Journal of Environmental Analytical Chemistry*, vol. 100, pp. 1–19, 2020.

[62] M. F. M. Yusop, M. A. Ahmad, N. A. Rosli, and M. E. A. Manaf, "Adsorption of cationic methylene blue dye using microwave-assisted activated carbon derived from acacia wood: optimization and batch studies," *Arabian Journal of Chemistry*, vol. 14, no. 6, Article ID 103122, 2021.

[63] S. Singh, G. K. Sidhu, and H. Singh, "Removal of methylene blue dye using activated carbon prepared from biowaste precursor," *Indian Chemical Engineer*, vol. 61, no. 1, pp. 28–39, 2019.

[64] D. Pathania, S. Sharma, and P. Singh, "Removal of methylene blue by adsorption onto activated carbon developed from Ficus carica bast," *Arabian Journal of Chemistry*, vol. 10, Article ID S1445, 2017.

[65] K. Ghosh, N. Bar, A. B. Biswas, and S. K. Das, "Removal of methylene blue (aq) using untreated and acid-treated eucalyptus leaves and GA-ANN modelling," *Canadian Journal of Chemical Engineering*, vol. 97, no. 11, pp. 2883–2898, 2019.

[66] T. Ahmed, W. Noor, O. Faruk, M. Bhoumick, and M. Uddin, "Removal of methylene blue (MB) from waste water by adsorption on jackfruit leaf powder (JLP) in continuously stirred tank reactor," *Journal of Physics: Conference Series*, vol. 1086, 2018.

[67] A. Ullah, M. Zahoor, W. U. Din et al., "Removal of methylene blue from aqueous solution using black tea wastes: used as efficient adsorbent," *Adsorption Science and Technology*, vol. 2022, Article ID 5713077, 9 pages, 2022.

[68] A. Varmazyar, S. Sedaghat, and M. Khalaj, "Highly efficient removal of methylene blue by a synthesized TiO 2/montmorillonite-albumin nanocomposite: kinetic and isothermal analysis in water," *RSC Advances*, vol. 7, no. 59, Article ID 37214, 2017.

[69] M. Khodaie, N. Ghasemi, B. Moradi, and M. Rahimi, "Removal of methylene blue from wastewater by adsorption onto ZnCl2 activated corn husk carbon equilibrium studies," *Journal of Chemistry*, vol. 2013, Article ID 383985, 6 pages, 2013.

[70] A. Ahmad, N. Khan, B. S. Giri, P. Chowdhary, and P. Chaturvedi, "Removal of methylene blue dye using rice husk, cow dung and sludge biochar: characterization, application, and kinetic studies," *Bioresource Technology*, vol. 306, Article ID 123202, 2020.

[71] Y. Wang and R. Liu, "Comparison of characteristics of twenty-one types of biochar and their ability to remove multi-

heavy metals and methylene blue in solution," *Fuel Processing Technology*, vol. 160, pp. 55–63, 2017.

[72] R. Acosta, V. Fierro, A. Martinez de Yuso, D. Nabarlatz, and A. Celzard, "Tetracycline adsorption onto activated carbons produced by KOH activation of tyre pyrolysis char," *Chemosphere*, vol. 149, pp. 168–176, 2016.

[73] A. A. Ceyhan, Ö. Şahin, C. Saka, and A. Yalçın, "A novel thermal process for activated carbon production from the vetch biomass with air at low temperature by two-stage procedure," *Journal of Analytical and Applied Pyrolysis*, vol. 104, pp. 170–175, 2013.

[74] N. Bouchemal, M. Belhachemi, Z. Merzougui, and F. Addoun, "The effect of temperature and impregnation ratio on the active carbon porosity," *Desalination and Water Treatment*, vol. 10, no. 1-3, pp. 115–120, 2009.

[75] S. Valliammai, Y. Subbareddy, K. Nagaraja, and B. Jeyaraj, "Removal of Methylene Blue from aqueous solution by activated carbon of Vigna mungo L and Paspalum scrobiculatum: equilibrium, kinetics and thermodynamic studies," *Journal of Chemical and Pharmaceutical Research*, vol. 8, 2017.

[76] M. S. Muzarpar, A. Lemana, K. Rahmanb, N. Maghporc, N. N. M. Hassana, and N. Misdana, "The adsorption mechanism of activated carbon and its application-A," *Institute for Research on Innovation and Industrial System (IRIS)*, vol. 1, no. 3, pp. 118–124, 2020.

[77] J.-j. Gao, Y.-b. Qin, T. Zhou et al., "Adsorption of methylene blue onto activated carbon produced from tea (Camellia sinensis L.) seed shells: kinetics, equilibrium, and thermodynamics studies," *Journal of Zhejiang University - Science B*, vol. 14, no. 7, pp. 650–658, 2013.

[78] G. Y. Abate, A. N. Alene, A. T. Habte, and D. M. Getahun, "Adsorptive removal of malachite green dye from aqueous solution onto activated carbon of Catha edulis stem as a low cost bio-adsorbent," *Environmental Systems Research*, vol. 9, no. 1, p. 29, 2020.

[79] T. Unugul and F. U. Nigiz, "Preparation and characterization an active carbon adsorbent from waste Mandarin peel and determination of adsorption behavior on removal of synthetic dye solutions," *Water, Air, & Soil Pollution*, vol. 231, no. 11, 2020.

[80] A. Ilnicka, J. Okonski, A. W. Cyganiuk, J. Patyk, and J. P. Lukaszewicz, "Zinc regarding the utilization of waste tires by pyrolysis," *Polish Journal of Environmental Studies*, vol. 25, no. 6, pp. 2683–2687, 2016.

[81] F. A. López, T. A. Centeno, F. J. Alguacil, and B. Lobato, "Distillation of granulated scrap tires in a pilot plant," *Journal of Hazardous Materials*, vol. 190, no. 1-3, pp. 285–292, 2011.

[82] A. Undri, B. Sacchi, E. Cantisani et al., "Carbon from microwave assisted pyrolysis of waste tires," *Journal of Analytical and Applied Pyrolysis*, vol. 104, pp. 396–404, 2013.

[83] M. Amirza, M. Adib, and R. Hamdan, "Application of agricultural wastes activated carbon for dye removal–An overview," *MATEC web of conferences*, vol. 103, 2017.

[84] I. H. Ali and H. A. Alrafai, "Kinetic, isotherm and thermodynamic studies on biosorption of chromium (VI) by using activated carbon from leaves of Ficus nitida," *Chemistry Central Journal*, vol. 10, no. 1, p. 36, 2016.

[85] X. S. Wang, H. J. Lu, L. Zhu, F. Liu, and J. J. Ren, "Adsorption of lead (II) ions onto magnetite nanoparticles," *Adsorption Science and Technology*, vol. 28, no. 5, pp. 407–417, 2010.

[86] Z. Jankovská, M. Večeř, I. Koutník, and L. Matějová, "A case study of waste scrap tyre-derived carbon black tested for nitrogen, carbon dioxide, and cyclohexane adsorption," *Molecules*, vol. 25, no. 19, 2020.

[87] A. H. Jawad, R. A. Rashid, M. A. M. Ishak, and K. Ismail, "Adsorptive removal of methylene blue by chemically treated cellulosic waste banana (Musa sapientum) peels," *Journal of Taibah University for Science*, vol. 12, no. 6, pp. 809–819, 2018.

[88] R. Ben Arfi, S. Karoui, K. Mougin, and A. Ghorbal, "Cetyltrimethylammonium bromide-treated Phragmites australis powder as novel polymeric adsorbent for hazardous Eriochrome Black T removal from aqueous solutions," *Polymer Bulletin*, vol. 76, no. 10, pp. 5077–5102, 2019.

[89] R. Wang, X.-W. Fan, and Y.-Z. Li, "Efficient removal of a low concentration of Pb (II), Fe (III) and Cu (II) from simulated drinking water by co-immobilization between low-dosages of metal-resistant/adapted fungus Penicillium janthinillum and graphene oxide and activated carbon," *Chemosphere*, vol. 286, Article ID 131591, 2022.

[90] S. Wang, Y.-R. Lee, Y. Won et al., "Development of high-performance adsorbent using KOH-impregnated rice husk-based activated carbon for indoor CO2 adsorption," *Chemical Engineering Journal*, vol. 437, Article ID 135378, 2022b.